electronics

MDPI

Article

A Study of Mutual Coupling Suppression between Two Closely Spaced Planar Monopole Antenna Elements for 5G New Radio Massive MIMO System Applications

Rao Shahid Aziz [1,*], Slawomir Koziel [1,2], Leifur Leifsson [3] and Stanislaw Szczepanski [2]

[1] Department of Engineering, Reykjavik University, 101 Reykjavik, Iceland; koziel@ru.is
[2] Faculty of Electronics, Telecommunications and Informatics, Gdansk University of Technology, 80-233 Gdansk, Poland; stanislaw.szczepanski@pg.edu.pl
[3] School of Aeronautics and Astronautics, Purdue State University, West Lafayette, IN 47907, USA; leifur@purdue.edu
* Correspondence: raos@ru.is; Tel.: +354-731-2152

Abstract: 5G NR (new radio) introduces the concept of massive MIMO (multiple-input multiple-output) technology, in which a larger number of antenna arrays are installed on the transceiver. Due to the increased number of antenna elements allocated close to each other (approximately at a distance of half a wavelength), mutual coupling becomes a serious problem leading to performance degradation of the MIMO communication system. In this communication, two different configurations of closely spaced antenna array elements are studied. In order to reduce the mutual coupling, a combination of a metamaterial-based frequency-selective surface (FSS), a metallic strip, and a slot element in the ground plane is examined. It is found that the proposed technique significantly suppresses mutual coupling from −12 dB to −25 dB. Both designs are fabricated and experimentally validated. The simulation results are in good agreement with the measurements. The proposed mutual coupling reduction technique may be suitable for massive MIMO systems in fifth-generation (5G) new radio applications.

Keywords: 5G NR; FSS; isolation; massive MIMO; mutual coupling; metamaterial; transceiver

Citation: Aziz, R.S.; Koziel, S.; Leifsson, L.; Szczepanski, S. A Study of Mutual Coupling Suppression between Two Closely Spaced Planar Monopole Antenna Elements for 5G New Radio Massive MIMO System Applications. *Electronics* **2023**, *12*, 2630. https://doi.org/10.3390/electronics12122630

Academic Editors: Dejan Drajic, Philipp Svoboda and Zoran Cica

Received: 16 May 2023
Revised: 6 June 2023
Accepted: 9 June 2023
Published: 12 June 2023

1. Introduction

Multiple-input multiple-output [1] technology (MIMO) is a well-established wireless communications technique for sending and receiving multiple data signals simultaneously over the same radio channel. MIMO techniques play a vital role in Wi-Fi communication, including in the 3G, 4G, and 4G LTE networks. Massive MIMO is an important technology in 5G NR, enhancing reliability and data rates in challenging environments [2]. This involves the application of MIMO on a larger scale in order to obtain greater network coverage and capacity. Massive MIMO employs many more transmitting and receiving antennas to increase the transmission gain and the spectral efficiency [3].

Cell-free massive MIMO with a multi-antenna user concept, in which a large number of distributed devices can communicate with the central processing unit (CPU), has gained attention recently for serving a small number of users at the same time–frequency resources block. It remarkably helps in enhancing gain and spectral efficiency [4]. When the multiple antennas are implemented in the MIMO system, the antenna elements are placed physically close to each other, and the effects of their mutual coupling become more pronounced [5,6]. The mutual coupling between two closely arranged antenna elements occurs due to (i) the flow of a surface current from the port excitation area, (ii) the space radiation, and (iii) the surface waves. Consequently, suppressing the mutual coupling within the miniaturized printed antenna elements becomes a greater challenge in the design of a 5G NR massive MIMO multi-antenna system.

The literature offers several techniques for mutual coupling reduction, including incorporation of electromagnetic bandgap (EBG) structures [7–9], defected ground structures (DGS) [10–12], decoupling networks [13–16], a complementary split-ring resonator (CSRR) [17,18], neutralization lines [19,20], metamaterials [21–23], and parasitic or slot elements [24–26].

The EBG structure can transmit, block, or pass specific electromagnetic (EM) waves. Basically, it acts as a low/high pass, stopband, or a bandpass filter. In [7], the authors propose a novel EBG unit cell and place it in between dual-polarized phased-array antenna elements to reduce mutual coupling. The mutual coupling between two microstrip patch antennas is suppressed using a modified electromagnetic bandgap decoupling structure in [8]. The patch antennas operate at an UWB between 3.1 GHz and 13.5 GHz. The MEBG is employed on the other side of the patch antennas and connected to the ground plane. Likewise, in [9], a uniplanar EBG presents mutual coupling reduction between elements of an UWB MIMO antenna. In [10], UWB MIMO antennas are utilized, and mutual coupling is suppressed by using a defected ground structure. The proposed UWB antenna covers the 2 GHz to 10 GHz band. Introducing arcs on the patch of the monopoles and on the ground plane enhances the performance of an antenna system and increases the mutual impedance among elements. The authors in [11] propose a two-port antenna which comprises a three-layer structure. Rectangular-shape defects in the ground plane are introduced to enhance the isolation between the two antenna ports. In [12], the authors propose compact MIMO antenna systems with improved isolation for sub-6 GHz 5G applications. The isolation is improved by introducing a T-shaped ground stub between the two elements. The antenna system operates at 3.6 GHz.

Utilization of decoupling networks is another technique for mutual coupling reduction in MIMO systems [13–16]. In [13], a two-substrate integrated waveguide (SIW) antenna array is proposed. A decoupling feed network is composed of a two-layer directional coupler which is connected to SIW slot antenna arrays. The results show good performance with coupling being about -35 dB at the center frequency. In [16], a decoupling device referred to as a cascaded power dividing decoupling network (C-PDDN) is proposed. It is cascaded between two radiators, to reduce the mutual coupling. It consists of two power dividers, two transmission lines, and one reactive component. The proposed methodology shows that the mutual coupling is suppressed over 20 dB. A CSRR [17,18] is a periodic or non-periodic structure. It is used to achieve both filtering and isolation improvement. The proposed antenna array of 1×2 array elements is composed of microstrip patches with a pair of CSRRs placed on the ground plane to reduce the coupling between the two patches. A -30 dB isolation band is achieved at 9.34 GHz to 9.45 GHz.

A novel neutralization line with decoupling network (NLDN) is proposed in [19] for wideband multi-element antenna arrays. A decoupling network is established between ports, and a neutralization line is introduced between the antenna arrays. The simulation and measured result show 20 dB isolation between the array elements. An approach based on a fractal isolator using an electromagnetic bandgap structure based on metamaterial for mutual coupling reduction in antenna arrays is proposed in [22]. With this technique, 37, 21, 20, and 31 dB isolation is achieved in the X-, Ku-, K-, and Ka-bands, respectively. In [24], a 4G/5G MIMO antenna is proposed for handphone application. Four antennas are implemented, and the isolation is improved by making slots between them. It gives about 15 dB isolation improvement in the 4G and 5G bands. In [26], mutual coupling is reduced using T-shape parasitic elements between two elements. It cancels the surface current effect and reduces the mutual coupling. The results show that 15 dB mutual coupling is diminished by this method.

Mobile communication technology is continuously advancing and involves massive MIMO systems as the novel solutions that need to be implemented in base transceiver systems. As elaborated on above, multi-antenna elements in the transceiver system raise the significant problem of mutual coupling between the closely spaced elements, degrading the overall system performance. This work proposes and investigates a mutual coupling

suppression technique which capitalized on some of the aforementioned approaches in an unconventional manner. More specifically, a metamaterial-based periodic FSS is combined with a metallic wall and placed between the two planar monopoles. Furthermore, the isolation is improved by creating a slot element on the common ground plane of the antenna elements. The proposed isolation technique is applied on two different configurations of an MIMO antenna system. In this investigation, first, the FSS unit cell is characterized in CST Microwave studio. The FSS wall, combining six novel unit cells, acts as a bandstop filter with the operating bandwidth covering the target frequency band of 24 GHz to 27 GHz. It is then combined with the metallic strip on the same substrate. Finally, a slot element 1 mm in width is etched on the ground plane of the MIMO system. As a result, an improved isolation is achieved between the closely spaced elements.

The originality and the technical contributions of the paper can be summarized as follows: (i) development of a novel frequency-selective surface (FSS) design for bandstop filtering purposes, (ii) development of a novel isolation wall combining the FSS and a metal strip to reduce mutual coupling among closely spaced array elements, (iii) development of a complete isolation enhancement structure consisting of several components not employed before in this combination, leading to excellent performance not reported before, (iv) numerical and experimental demonstration of the applicability of the proposed technique to various MIMO system architectures at mmWave frequencies, (v) demonstration of the superiority of the considered approach over state-of-the-art methods available in the literature.

2. Case Study: Closely Spaced mmWave MIMO Systems

This section describes two different design configurations of an MIMO system of two closely spaced monopole antennas. Both designs operate in the millimeter wave band. The primary point of interest is a reduction in mutual coupling between the antenna elements, with the specific FSS-based technique proposed and elaborated on later in the paper.

2.1. Design 1

Figure 1 shows the geometry of two identical monopole antennas sharing a common ground plane and dielectric material. The monopoles are individually excited through the probe feeds. In this design configuration, both monopoles are facing the +z-direction. The center-to-center distance between the two monopoles is 6.25 mm (0.535λ), whereas the edge-to-edge distance is 1.25 mm (0.107λ), where λ is the free-spaced wavelength at 25.5 GHz (center frequency). The monopole design is imprinted on Rogers RO4003 (lossy) dielectric material with relative permittivity ε_r = 3.38, thickness t = 0.508 mm, and dissipation factor tanδ = 0.0027. The common dielectric substrate is also Rogers RO4003 (lossy), but the substrate thickness is 1.524 mm to ensure improved rigidness of the structure. Figure 2 illustrates the reflection and transmission coefficients for Design 1, which indicate the level of mutual coupling between the two monopoles; it ranges from −12 to −23 dB within the frequency range of interest (24 GHz to 27 GHz).

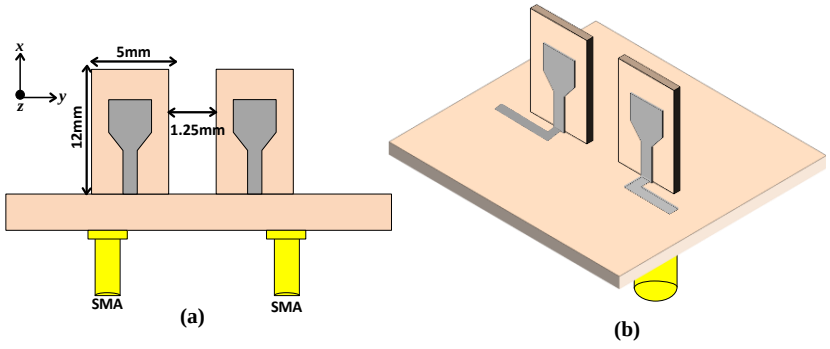

Figure 1. *Cont.*

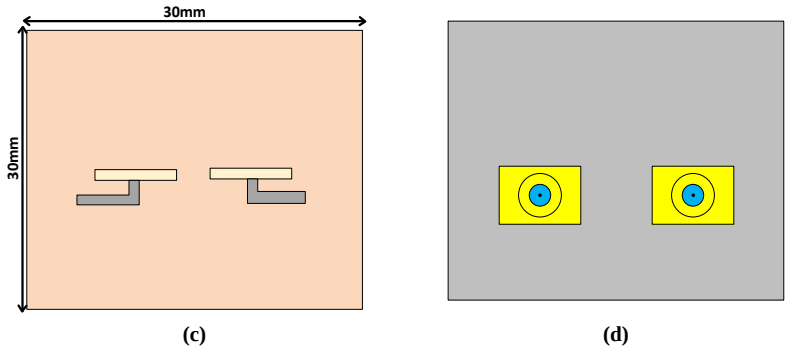

Figure 1. Geometry configuration for Design 1: (**a**) side view, (**b**) perspective view, (**c**) top view, (**d**) bottom view.

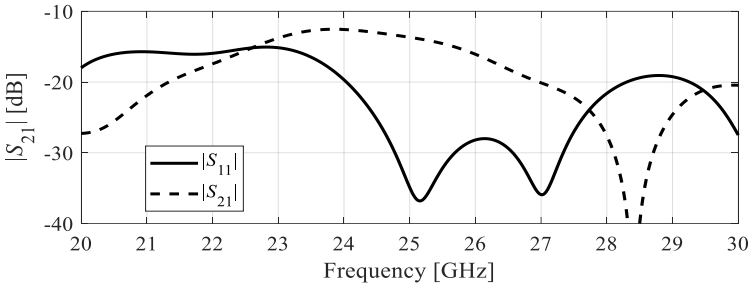

Figure 2. Reflection and transmission coefficients for Design 1.

2.2. Design 2

The second design is shown in Figure 3. It also consists of two identical monopole antennas sharing a common ground plane and dielectric material. Both monopoles are individually fed via probe feeds. However, here, the monopoles are facing the opposite directions, i.e., +z and −z. The dimensions and the substrate materials are the same as for Design 1. Figure 4 shows the reflection and transmission coefficients for Design 2. The mutual coupling ranges from −9 to −16 dB within the frequency range of interest (24 GHz to 27 GHz).

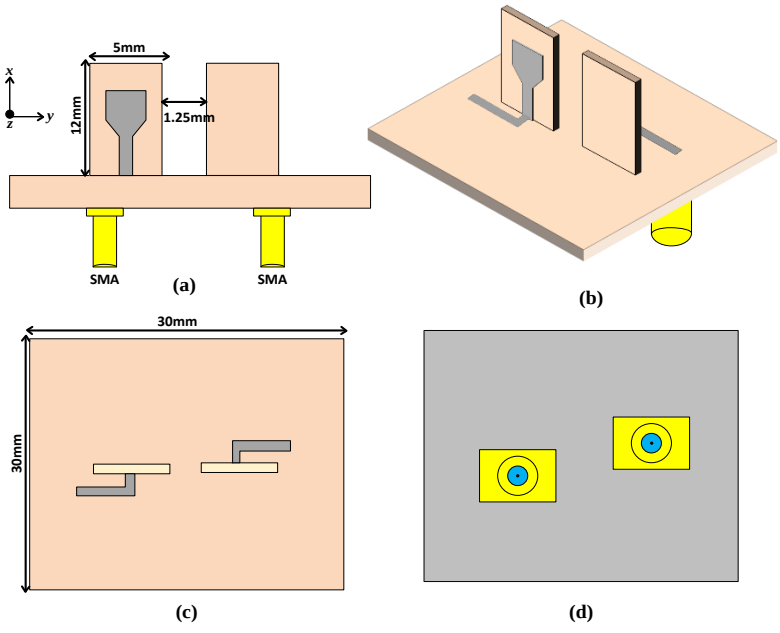

Figure 3. Geometry configuration for Design 2: (**a**) side view, (**b**) perspective view, (**c**) top view, (**d**) bottom view.

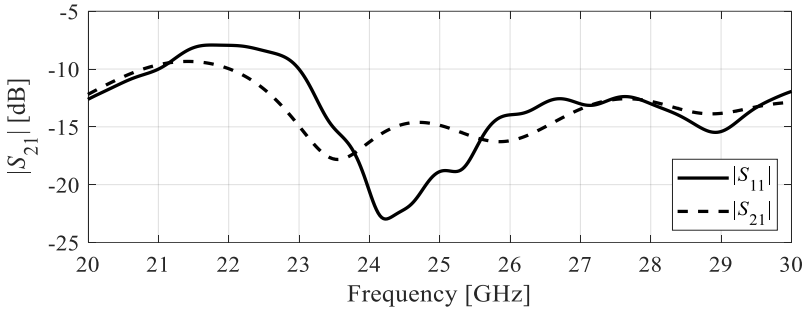

Figure 4. Reflection and transmission coefficients for Design 2.

3. Mutual Coupling Suppression using Frequency-Selective Surface

This section describes the mutual coupling reduction technique proposed in this work. It is explained using several design case studies. The major components of the presented approach are isolation improvements using a frequency-selective surface (FSS), a FSS with a metallic strip, and the ground slot.

3.1. Frequency-Selective Surface: Unit Cell

Frequency-selective surfaces (FSSs) are arrays of periodic elements consisting of metallic layers imprinted on dielectric material. FSSs exhibit bandpass or bandstop characteristics depending on the arrangement of their unit cells. FSSs are widely used as spatial filters, but most of them feature a narrow operating band. In this work, a broadband FSS is designed which acts as a bandstop filter in the millimeter wave frequency range. The FSS unit cell consists of two metallic layers imprinted on both sides of a dielectric material. The FSS is designed on a Rogers RO4003C (lossy) dielectric material with material thickness t = 0.508 mm, relative permittivity ε_r = 3.38, and dissipation factor tanδ = 0.0027. The unit cell geometry consists of two cross-shape dipoles enclosed in a circle.

Figure 5 shows the FSS geometry, which consists of two well-known shapes, i.e., two crossed dipoles, and an outer ring printed on both sides of the FSS unit cell. The transmission coefficient corresponding to the two crossed dipoles exhibits a stopband from 40.1 to 46.4 GHz below −10 dB, as indicated in Figure 6a. Likewise, an outer ring yields a stopband transmission from 20 GHz to 38.51 GHz (again, at the −10 dB level). When both shapes are combined, two broad stopbands are obtained in the range from 22.28 GHz to 55.78 GHz below −10 dB, as also shown in Figure 6. The stopband of the proposed FSS can be further enhanced through a parametric study of the combined unit cell parameters (Ri and L). A procedure for rigorous optimization of the unit cell is also applied to achieve a broad stopband. The FSS unit cell is characterized using the frequency domain solver of CST Microwave Studio, using Floquet ports and periodic boundary conditions. Its transmission and reflection coefficients are shown in Figure 6. Table 1 provides the optimized values of the unit cell parameters.

Table 1. Proposed FSS unit cell dimensions.

Parameters	Quantities (Millimeters)
P	4.24
W	0.1
L	0.45
Ri	0.72
Ro	1.85

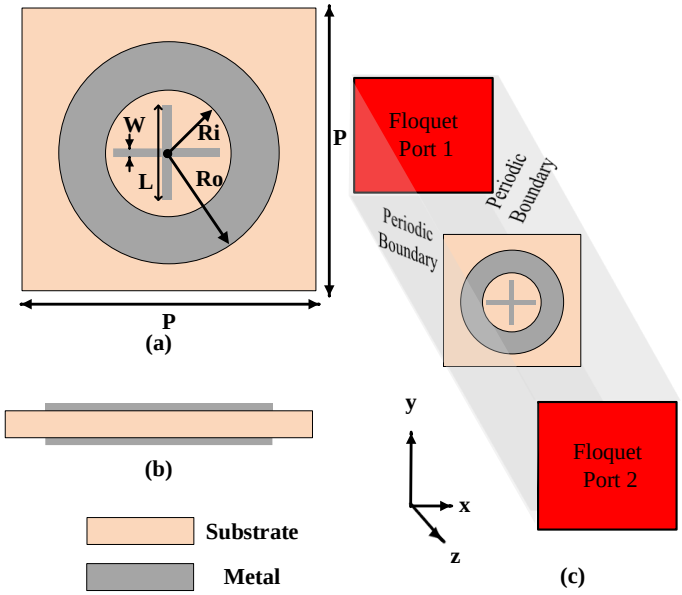

Figure 5. Proposed FSS unit cell geometry, (**a**) top view, (**b**) side view, (**c**) unit cell characterization in CST with Floquet ports and periodic boundary conditions.

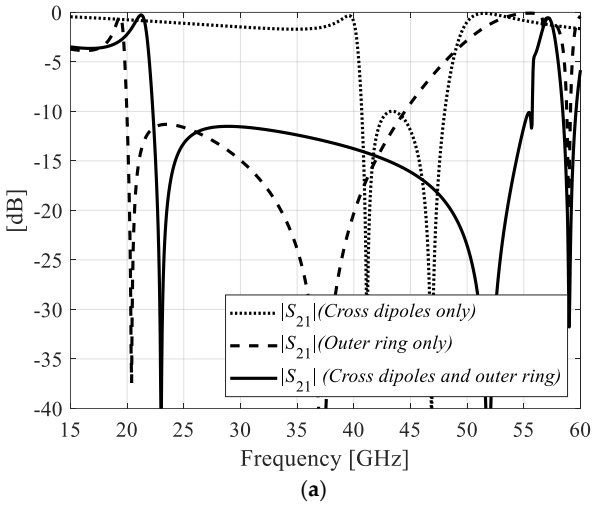

Figure 6. Simulated transmission and reflection coefficients of the proposed FSS unit cell, (**a**) S_{21}, (**b**) S_{11}.

3.2. Frequency-Selective Surface for Mutual Coupling Reduction

The proposed FSS can be used to reduce mutual coupling between the two monopole antennas. For that purpose, six FSS unit cells are combined into a wall and placed between the closely spaced elements. Figure 7a–d shows the wall geometry. Its total size is 12.70 mm × 19.08 mm. Figures 8 and 9 show the effect of the FSS wall for the case of Design 1. The isolation is improved from −12 dB to −20 dB in the desired frequency band. Similarly, the FSS wall applied to Design 2 improves the isolation from −15 dB to −21 dB.

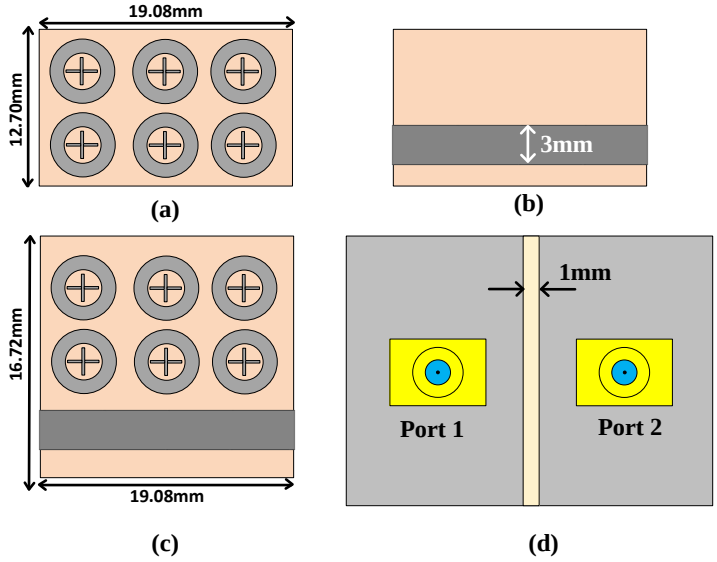

Figure 7. FSS-based isolation wall: (**a**) arrangement of FSS unit cells, (**b**) metallic strip, (**c**) FSS and metallic wall, (**d**) ground plane slot.

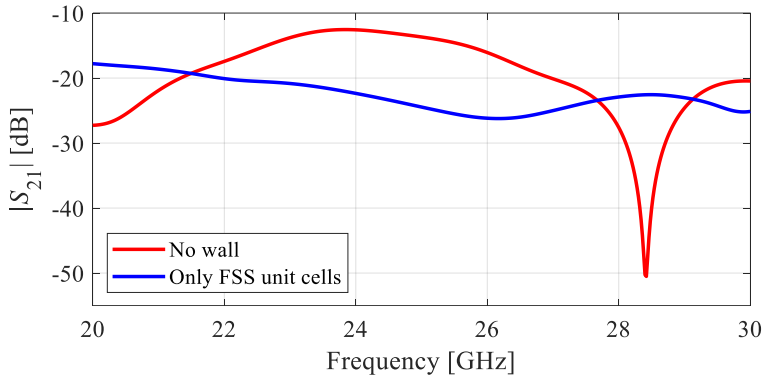

Figure 8. Transmission coefficient of Design 1 with FSS unit cells only.

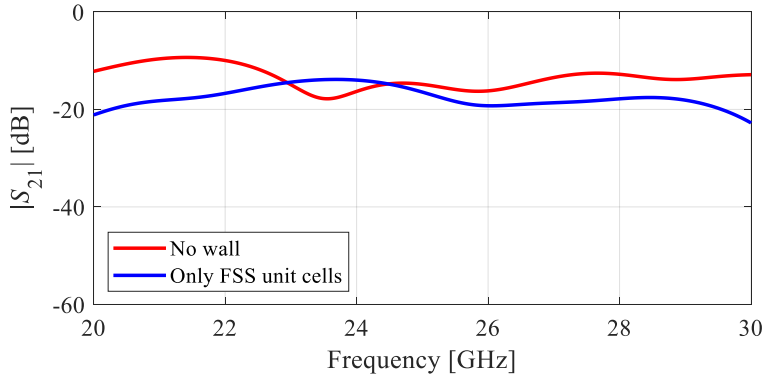

Figure 9. Transmission coefficient of Design 2 with FSS unit cells only.

3.3. FSS Wall and Metallic Strip

The proposed isolation can be further improved by adding a 3 mm metallic strip beneath the FSS wall. With this enhancement, the total size of the FSS becomes 16.72 mm × 19.08 mm. Figure 10 shows that isolation in Design 1 is improved from −20 dB to −33 dB in certain regions of the desired bands. On the other hand, Design 2 exhibits consistent isolation improvement in the entire desired band (below −25 dB), as indicated in Figure 11.

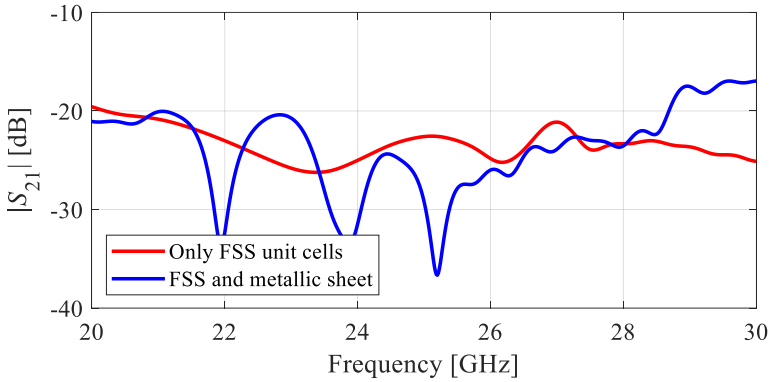

Figure 10. Transmission coefficient of Design 1 with FSS unit cells and metallic strips.

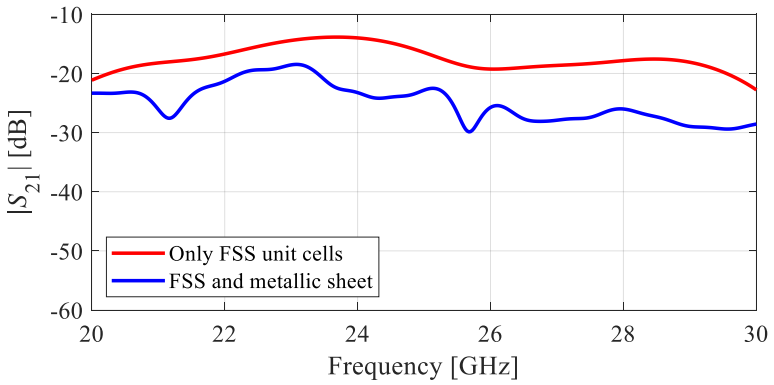

Figure 11. Transmission coefficient of Design 2 with FSS unit cells and metallic strips.

3.4. Ground Slot

Finally, a 1 mm slot in the ground plane is introduced for further isolation improvement. It can be seen that mutual coupling is significantly suppressed for both MIMO designs. For Design 1, the isolation is now below −25 dB (cf. Figure 12), whereas, for Design 2, the isolation is below −28 dB, as reported in Figure 13.

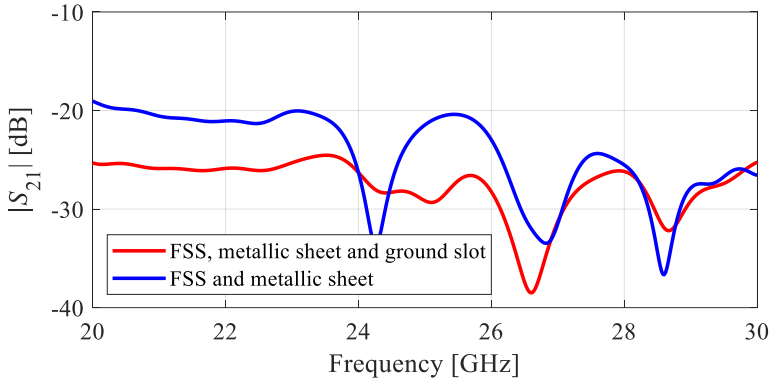

Figure 12. Transmission coefficient of Design 1 with FSS unit cells, metallic strips, and ground slot.

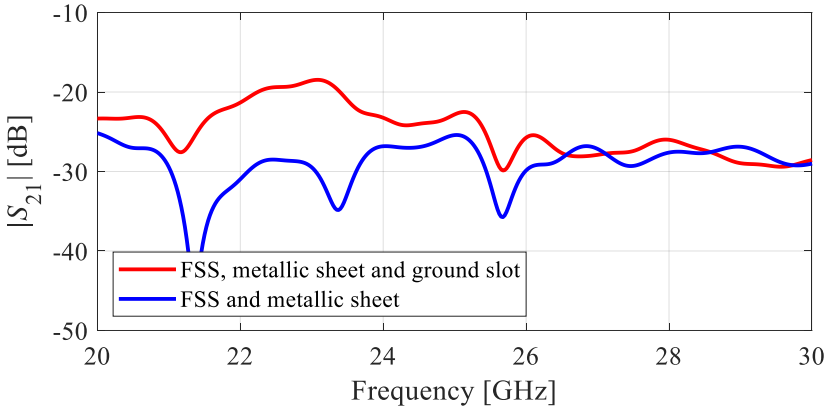

Figure 13. Transmission coefficient of Design 2 with FSS unit cells, metallic strips, and ground slot.

The CST simulation setups for Designs 1 and 2 are shown in Figure 14. The overall simulated results for all the applied techniques of both designs are shown in Figures 15 and 16, respectively. Furthermore, as shown in Figure 17, using the surface current distributions, the proposed isolation improvement technique suppresses the coupling between the two ports sharing a common ground plane.

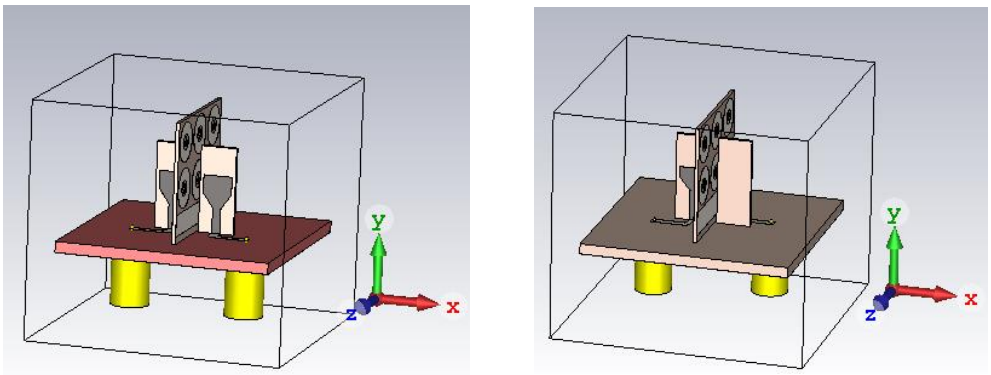

(**a**) (**b**)

Figure 14. CST simulation setups for (**a**) Design 1, and (**b**) Design 2.

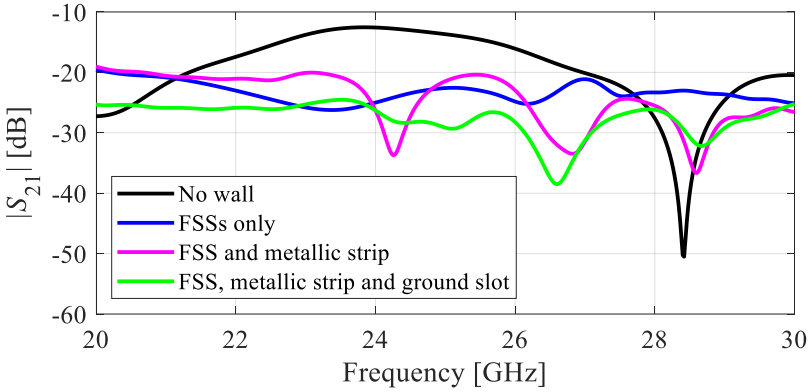

Figure 15. Transmission coefficients of Design 1: no wall, FSS wall, FSSs and metallic wall, FSSs, metallic wall, and ground slot.

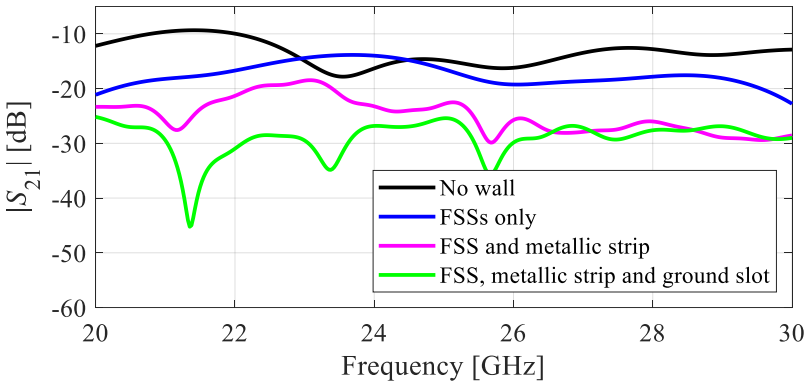

Figure 16. Transmission coefficients of Design 2: no wall, FSS wall, FSSs and metallic wall, FSSs, metallic wall, and ground slot.

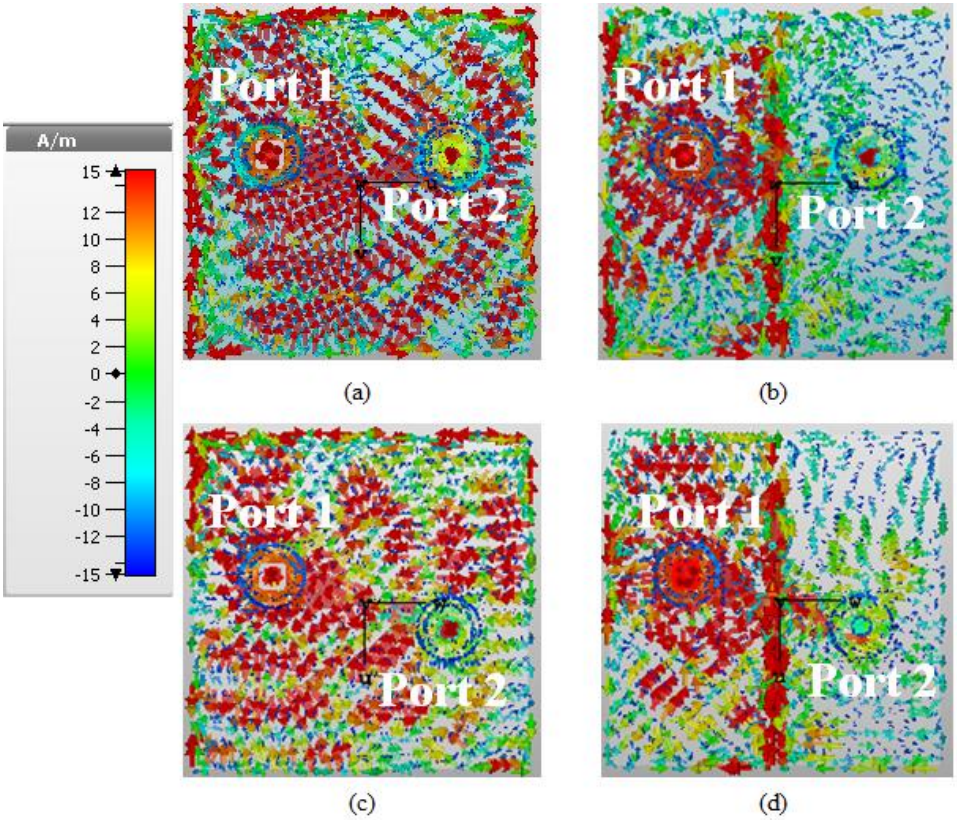

Figure 17. Surface current distributions: Design 1 without (**a**) and with (**b**) the proposed mutual coupling suppression structure; Design 2 without (**c**) and with (**d**) the mutual coupling suppression structure.

4. Working Principle

The closely spaced antennas in an MIMO system radiate electromagnetic (EM) waves in free space and on its ground. This causes an increase in mutual coupling. In order to reduce this effect, the FSS unit cell acts as a stopband filter, showing a wide stopband of 33.5 GHz.

The combination of the FSS stopband filter blocks the unwanted EM waves from the neighboring mounted antenna element in the MIMO system, which leads to isolation improvement in both designs. However, there is more room for improvement. Therefore, a metallic wall beneath the FSS unit cells and the slot on the shared ground plane is implemented. The metallic strip helps in the prevention of air coupling, whereas the ground slot aids in the separation of the elements from each other. This combination further

enhances the isolation in the MIMO system design. The actual gain in Design 1 before adding the proposed isolation structure is 4.55 dBi, and, after adding the aforementioned structure, it rises to 6.32 dBi. Similarly, the actual gain in Design 2 before adding the proposed structure is 4.99 dBi, and, after adding the FSS wall, it becomes 6.47 dBi.

5. Experimental Validation and Benchmarking

This section provides experimental validation of both the MIMO designs considered earlier in this section. Measurement data are compared with the EM simulation results.

5.1. Experimental Validation of Design 1

The prototype of Design 1 including the FSS wall and the remaining components as described earlier is shown in Figures 11b and 18a. The S-parameters of the MIMO system are tested using the 10 MHz to 40 GHz vector network analyzer PNA-X N5242A (Agilent Technologies, Santa Clara, CA, USA). Figure 18c shows the comparison between the simulated and measured S-parameters. It can be seen that the measured mutual coupling is below −22 dB at 24 GHz, and it is further improved beyond 26 GHz, achieving less than −40 dB between 26.5 GHz and 27 GHz. The discrepancies between the two data sets, especially noticeable in the 24 GHz to 25.5 GHz frequency range, result from the inaccuracies of the fabrication and manual assembly process. The FSS wall with metallic strip is inserted between the two monopole antennas using glue, which also contributes to the mentioned misalignments. The deviations of the electrical properties of the substrate material and the connector from their nominal values at millimeter wave frequencies constitute another reason for the discrepancies between the simulation and measurement data. A comparison of simulated and measured radiation patterns can be found in Figure 19. Also in this case, the agreement between the two data sets is satisfactory.

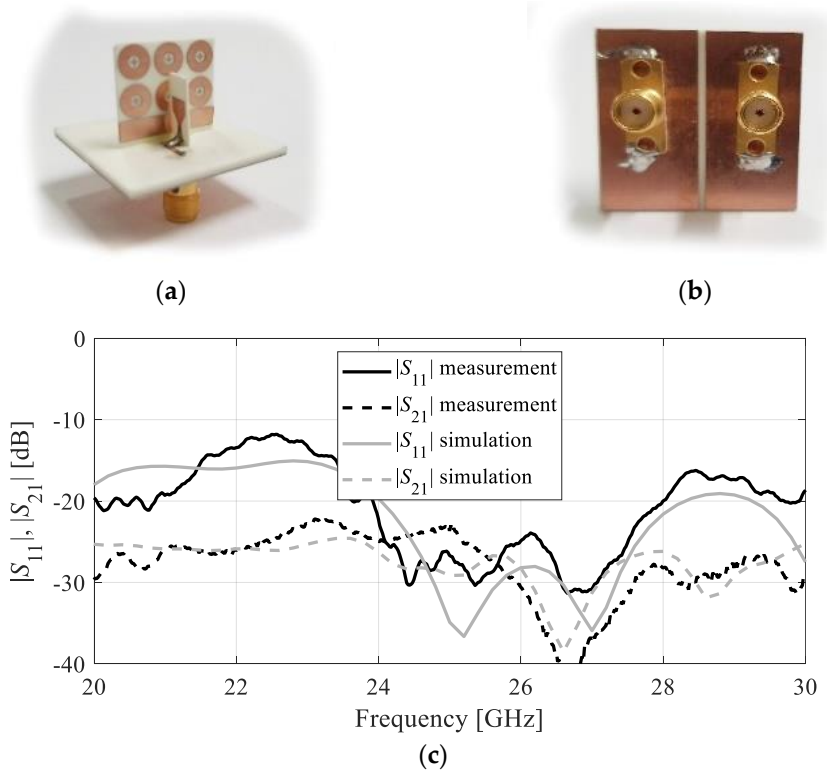

Figure 18. Fabricated prototype of Design 1, (**a**) perspective view, (**b**) back view, (**c**) simulated and measured S-parameters.

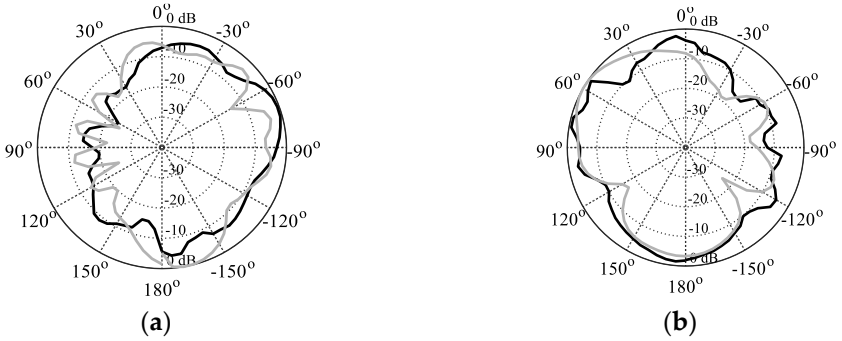

Figure 19. Design 1: simulated (gray) and measured (black) radiation patterns at 25.5 GHz: (**a**) H-plane, (**b**) E-plane.

5.2. Experimental Validation of Design 2

Design 2 is fabricated and tested using the same measurement setup. Figure 20a,b shows a photograph of the prototype with the FSS wall inserted between the two monopole antennas. Figure 20c shows the reflection and transmission coefficients of Design 2 along with the corresponding measurement data. It can be seen that both simulated and measured results are in reasonable agreement. The reflection coefficient is below −10 dB from 24 GHz to 27 GHz. The mutual coupling is −28 dB at 24 GHz and below −35 dB in the entire target frequency range. In this case, the discrepancies between the simulation and measurements are smaller, and their origin is of the same nature as explained in the previous section. Figure 21 provides a comparison of the simulated and measured radiation patterns.

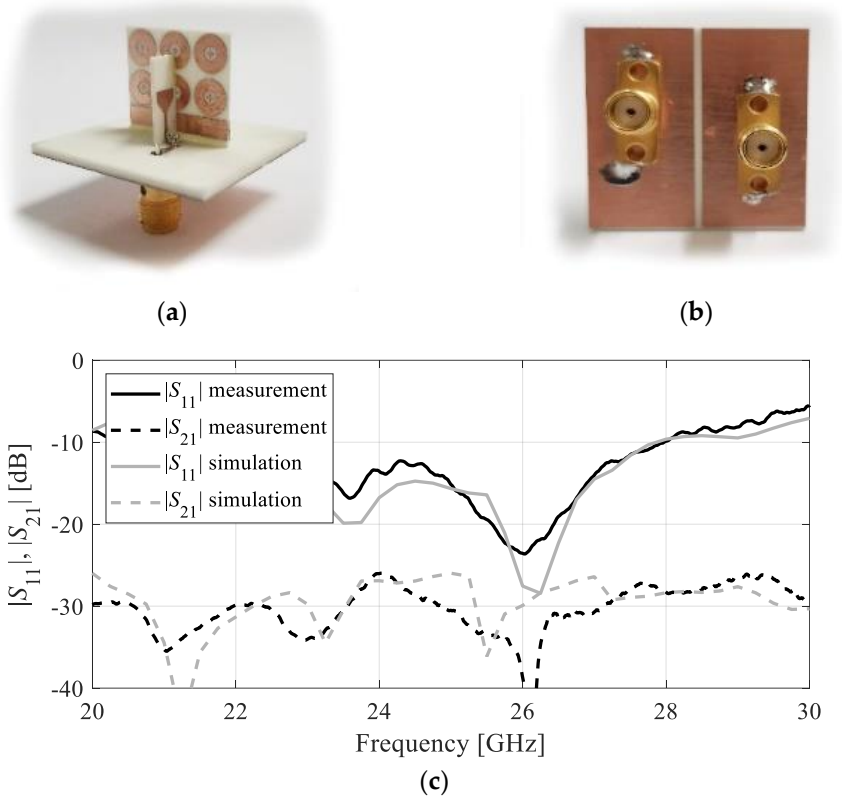

Figure 20. Fabricated prototype of Design 2, (**a**) perspective view, (**b**) back view, (**c**) simulated and measured S-parameters.

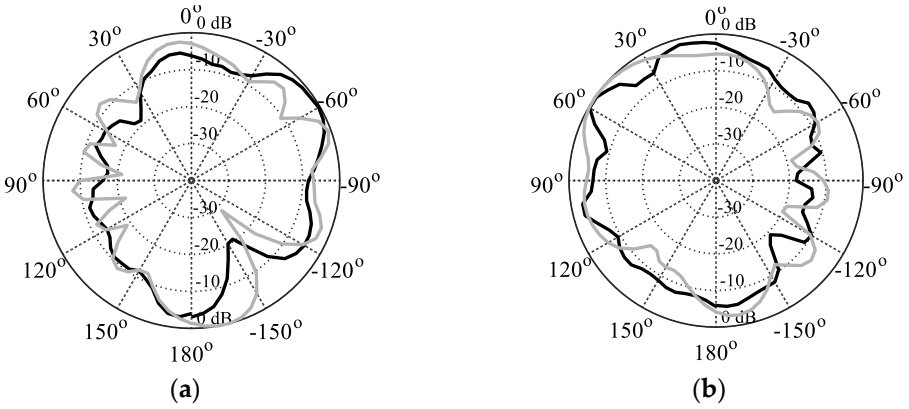

Figure 21. Design 2: simulated (gray) and measured (black) radiation patterns at 25.5 GHz: (**a**) H-plane, (**b**) E-plane.

6. Benchmarking

Table 2 shows the performance comparison of the proposed mutual coupling reduction technique versus that of state-of-the-art designs reported in the literature. The comparison is conducted in terms of the arrangement of the mutual coupling suppression technique, edge-to-edge element distance, and mutual coupling reduction in terms of $|S21|$.

Table 2. Performance comparison between the proposed mutual coupling reduction technique and state-of-the-art solutions.

Design	Mutual Coupling Structures	Operating Frequency (GHz)	Edge-to-Edge Spacing	Max. Mutual Coupling Suppression $\|S21\|$ (dB)	Total Size of the Antenna System
[8]	EBG	3.1 to 13.5	≈1.01λ	23	≈0.87 λ × 1.55 λ × 0.0008 λ
[10]	DGS	2 to 10	≈0.1λ	30	≈1.2 λ × 0.7λ × 0.032 λ
[16]	Cascaded decoupling network	2.3 to 2.4/2.4 to 2.483	≈0.18λ	20	≈0.82 λ × 0.82 λ × 0.25 λ
[19]	Neutralization line and decoupling network	4.68 to 5.5	≈0.083λ	20	Not available
[22]	EBG and metamaterial wall	8.7–11.7, 11.9–14.6, 15.6–17.1, 22–26, and 29–34.2	≈0.65λ	37, 21, 20, 20, and 31	≈0.96 λ × 0.96 λ × 0.18 λ
[27]	FSS wall	57 to 63	≈0.5λ	30	Not available
[28]	Metasurface	23.8 to 25.2	≈0.3λ	25	≈5.65 λ × 1.7 λ × 0.28 λ
[29]	Metasurface	28 and 39	≈0.23λ	30 and 48	≈0.7 λ × 0.63 λ × 0.013 λ
[30]	EBG	28 and 39	≈0.5λ	30 and 25	≈1.43 λ × 0.79 λ × 0.074 λ
This work (Design 1)	FSS, metallic strip, and ground slot	24 to 27	≈0.107λ	22.5	≈2.57λ × 2.57λ × 1.43λ
This work (Design 2)	FSS, metallic strip, and ground slot	24 to 27	≈0.107λ	22.5	≈2.57λ × 2.57λ × 1.43λ

Most available mutual coupling suppression studies consider lower operating frequencies, specifically, the sub-6 GHz range, and only very few papers address the issue at higher frequencies, in particular, at mmWave frequencies. The size of the MIMO antenna system becomes physically smaller at higher frequencies, and the antenna system is considerably more difficult to handle compared to at a lower frequency. Additionally, for massive MIMO antenna systems, the transmitting and receiving antennas are situated close to each other so that mutual coupling effects degrade the overall performance of the system to a great extent. The solution proposed in this work addresses these specific issues, i.e., isolation improvement under challenging scenarios with physically small MIMO systems where the application of a single technique is typically insufficient (recall that the approach presented here combines three methods: FSS unit cells with a metal strip wall and a slot on the common ground plane). Bearing this in mind, the performance of our technique is superior in terms of offering a significant reduction in mutual coupling while operating under a small edge-to-edge radiator spacing of only about 0.1λ. It is better than what is proposed in, e.g., [27], let alone the many solutions reported for lower operating frequencies, which are not easily transferrable to higher bands.

7. Conclusions

This communication proposes an isolation technique for closely spaced antenna elements in an MIMO system. A part of the presented approach is a novel wideband FSS unit cell, introduced to suppress the mutual coupling, with the specific realization being an FSS-based wall supplemented by a metallic strip, both inserted between the two antenna elements. Furthermore, a slot is etched in the common ground plane to reduce the surface current between the two antennas. A detailed study of the effects of the proposed approach on the mutual coupling level is carried out to corroborate its efficacy using two specific examples of MIMO systems, referred to as Design 1 and Design 2. It is demonstrated, both numerically and experimentally, that the proposed technique improves the isolation by about 23 dB and 30 dB for Designs 1 and 2, respectively. The presented mutual coupling suppression technique provides an attractive alternative to existing approaches and can be used in the design of compact platforms with high isolation for 5G NR massive MIMO system applications.

Author Contributions: Conceptualization, R.S.A.; methodology, R.S.A. and S.K.; software, R.S.A. and S.K.; validation, R.S.A. and L.L.; formal analysis, R.S.A.; investigation, R.S.A. and S.K.; resources, L.L. and S.S.; data curation, R.S.A. and S.K.; writing—original draft preparation, R.S.A. writing—review and editing, S.K. and L.L.; visualization, R.S.A. and S.K.; supervision, S.S.; project administration, L.L.; funding acquisition, S.S. All authors reviewed the manuscript. All authors have read and agreed to the published version of the manuscript.

Funding: The authors would like to thank Dassault Systemes, France, for making CST Microwave Studio available. This work is partially supported by the Icelandic Centre for Research (RANNIS) Grant 174573 and by National Science Centre of Poland grant 2020/37/B/ST7/01448.

Data Availability Statement: All data generated or analyzed during this study are included in this published article.

Acknowledgments: The authors thank Dassault Systemes, France, for making CST Microwave Studio available.

Conflicts of Interest: The authors declare no conflict of interest. The funders had no role in the design of the study; in the collection, analyses, or interpretation of data; in the writing of the manuscript; or in the decision to publish the results.

References

1. Oestges, C.; Guillaud, M.; Debbah, M. Multi-polarized MIMO communications: Channel model, mutual information and array optimization. In Proceedings of the 2007 IEEE Wireless Communications and Networking Conference, Hong Kong, China, 11–15 March 2007; pp. 1057–1061.
2. Khan, M.F.; Pesch, D. On Performance of multi-user Massive MIMO for 5G and beyond. In Proceedings of the IEEE 95th Vehicular Technology Conference: (VTC2022-Spring), Helsinki, Finland, 19–22 June 2022; pp. 1–5.
3. Zhang, J.; Chen, S.; Lin, Y.; Zheng, J.; Ai, B.; Hanzo, L. Cell-free massive MIMO: A new next-generation paradigm. *IEEE Access* **2019**, *7*, 99878–99888. [CrossRef]
4. Zhou, M.; Li, J.; Xie, M.; Zhang, C.; Yuan, J. Average Sum Rate of D2D Underlaid Multigroup Multicast Cell-Free Massive MIMO With Multi-Antenna Users. *IEEE Wirel. Commun. Lett.* **2023**, *12*, 60–64. [CrossRef]
5. Pei, T.; Zhu, L.; Wang, J.; Wu, W. A Low-Profile Decoupling Structure for Mutual Coupling Suppression in MIMO Patch Antenna. *IEEE Trans. Antennas Propag.* **2021**, *69*, 6145–6153. [CrossRef]
6. Bhattacharjee, S.; Ghosh, C.K. Deployment of Frequency Selective Surface (FSS) for Reduction of Mutual Coupling and Cross-Polarization in MIMO Antennas. In Proceedings of the International Interdisciplinary Conference on Mathematics, Engineering and Science (MESIICON), Durgapur, India, 11–12 November 2022; pp. 1–5.
7. Benny, S.; Sahoo, S. Mutual Coupling Reduction between elements of Dual-polarization Phased Array Antenna for Weather Radars. In Proceedings of the 24th International Microwave and Radar Conference (MIKON), Gdansk, Poland, 12–14 September 2022; pp. 1–6.
8. Fadehan, G.A.; Olasoji, Y.O.; Adedeji, K.B. Mutual Coupling Effect and Reduction Method with Modified Electromagnetic Band Gap in UWB MIMO Antenna. *Appl. Sci.* **2022**, *12*, 12358. [CrossRef]
9. Dabas, T.; Gangwar, D.; Kanaujia, B.K.; Gautam, A.K. Mutual coupling reduction between elements of UWB MIMO antenna using small size uniplanar EBG exhibiting multiple stop bands. *AEU Int. J. Electron. Commun.* **2018**, *93*, 32–38. [CrossRef]

10. Babu, K.V.; Anuradha, B. Design of UWB MIMO antenna to reduce the mutual coupling using defected ground structure. *Wirel. Pers. Comm.* **2021**, *118*, 3469–3484. [CrossRef]
11. Dash, J.C.; Sarkar, D. Microstrip Patch Antenna System with Enhanced Inter-Port Isolation for Full-Duplex/MIMO Applications. *IEEE Access* **2021**, *9*, 156222–156228. [CrossRef]
12. Saurabh, A.K.; Meshram, M.K. Compact sub-6 GHz 5G-multiple-input-multiple-output antenna system with enhanced isolation. *Int. J. RF Micro. Comp. Aided Eng.* **2020**, *30*, e22246. [CrossRef]
13. Diman, A.A. Efficient SIW-Feed Network Suppressing Mutual Coupling of Slot Antenna Array. *IEEE Trans. Antennas Propag.* **2021**, *69*, 6058–6063. [CrossRef]
14. Karmani, F.; Rezaei, P.; Ali Amn-e-Elahi, A.; Meiguni, J.S. A compact and wideband array antenna with efficient hybrid feed network. *Int. J. RF Microw. Comput. Aided Eng.* **2020**, *30*, e22393.
15. Ghannad, A.A.; Khalily, M.; Xiao, P.; Tafazolli, R.; Kishk, A.A. Enhanced matching and vialess decoupling of nearby patch antennas for MIMO system. *IEEE Antennas Wirel. Propag. Lett.* **2019**, *18*, 1066–1070. [CrossRef]
16. Li, M.; Wang, M.; Jiang, L.; Yeung, L.K. Decoupling of Antennas with Adjacent Frequency Bands Using Cascaded Decoupling Network. *IEEE Trans. Antennas Propag.* **2021**, *69*, 1173–1178. [CrossRef]
17. Kedze, K.E.; Zhou, W.; Javanbakht, N.; Xiao, G.; Shaker, J.; Amaya, R.E. Implementing Complementary Split Ring Resonators for Mutual Coupling Suppression in Dual Differentially-Fed Microstrip Patch Array Antenna. In Proceedings of the 2022 IEEE International Symposium on Phased Array Systems & Technology (PAST), Waltham, MA, USA, 11–14 October 2022.
18. Selvaraju, R.; Jamaluddin, M.H.; Kamarudin, M.R.; Nasir, J.; Dahri, M.H. Mutual Coupling Reduction and Pattern Error Correction in a 5G Beamforming Linear Array Using CSRR. *IEEE Access* **2018**, *6*, 65922–65934. [CrossRef]
19. Zou, X.-J.; Wang, G.-M.; Kang, G.-Q.; Song, W.; Tan, M.; Xu, X.-G.; Zhu, H. Wideband coupling suppression with neutralization-line-incorporated decoupling network in MIMO arrays. *AEU Int. J. Electron. Commun.* **2023**, *167*, 154688. [CrossRef]
20. Wu, T.; Wang, M.-J.; Chen, J. Decoupling of MIMO antenna array based on half-mode substrate integrated waveguide with neutralization lines. *AEU Int. J. Electron. Commun.* **2022**, *157*, 154416. [CrossRef]
21. Alibakhshikenari, M.; Salvucci, A.; Polli, G.; Virdee, B.S.; See, C.H.; Abd-Alhameed, R.; Limiti, E. Mutual coupling reduction using metamaterial supersubstrate for high performance & densely packed planar phased arrays. In Proceedings of the 2018 22nd International Microwave and Radar Conference (MIKON), Poznan, Poland, 14–17 May 2018.
22. Alibakhshikenari, M.; Khalily, M.; Virdee, B.S.; See, C.H.; Abd-Alhameed, R.A.; Limiti, E. Mutual Coupling Suppression Between Two Closely Placed Microstrip Patches Using EM-Bandgap Metamaterial Fractal Loading. *IEEE Access* **2019**, *7*, 23606–23614. [CrossRef]
23. Kumar, P.; Ali, T.; Pai, M.M.M. Electromagnetic Metamaterials: A New Paradigm of Antenna Design. *IEEE Access* **2021**, *9*, 18722–18751. [CrossRef]
24. Kumar, A.; Ansari, A.Q.; Kanaujia, B.K.; Kishor, J.; Matekovits, L. A review on different techniques of mutual coupling reduction between elements of any MIMO antenna. Part 1: DGSs and parasitic structures. *Radio Sci.* **2021**, *56*, e2020RS007122. [CrossRef]
25. Ikram, M.; Sharawi, M.S.; Shamim, A.; Sebak, A. A multiband dual-standard MIMO antenna system based on monopoles (4G) and connected slots (5G) for future smart phones. *Micro. Optic. Technol. Lett.* **2018**, *60*, 1468–1476. [CrossRef]
26. Faraz, F.; Li, Q.; Chen, X.; Abdullah, M.; Zhang, S.; Zhang, A. Mutual Coupling Reduction for Linearly Arranged MIMO Antenna. In Proceedings of the Cross Strait Quad-Regional Radio Science and Wireless Technology Conference (CSQRWC), Taiyuan, China, 18–21 July 2019; pp. 1–3.
27. Karimian, R.; Kesavan, A.; Nedil, M.; Denidni, T.A. Low-mutual-coupling 60-GHz MIMO antenna system with frequency selective Surface Wall. *IEEE Antennas Wirel. Propag. Lett.* **2017**, *16*, 373–376. [CrossRef]
28. Zhen, T.; Zhang, Z.; Wu, X. Design of millimeter wave array antenna decoupling construction based on metasurface. In Proceedings of the 2021 International Applied Computational Electromagnetics Society (ACES-China) Symposium, Chengdu, China, 28–31 July 2021; pp. 1–2.
29. Pawar, S.; Mastromatteo, S.; Yakovlev, A.B.; Bernety, H.M.; Skinner, H.G.; Suh, S.Y.; Alù, A. Elliptical Metasurface Cloaks for Decoupling and Cloaking of Microstrip Monopole Antennas at 28 GHz and 39 GHz for 5G Wireless Applications. In Proceedings of the 2020 IEEE International Symposium on Antennas and Propagation and North American Radio Science Meeting, Montreal, QC, Canada, 5–10 July 2020; pp. 805–806.
30. Thi, D.; Phuong, N.T.B.; Son, P.D.; Van Yem, V. Improving Characteristics of 28/38 GHz MIMO Antenna for 5G Applications by Using Double-Side EBG Structure. *J. Commun.* **2019**, *14*, 1–8.